Published in final edited form as:
J Am Chem Soc. 2010 November 3; 132(43): 15351–15358. doi:10.1021/ja106855m.

A Chelator-Free Multifunctional [^{64}Cu]-CuS Nanoparticle Platform for Simultaneous Micro-PET/CT Imaging and Photothermal Ablation Therapy

Min Zhou[†], **Rui Zhang**[†], **Miao Huang**[†], **Wei Lu**[†], **Shaoli Song**[†,‡], **Marites P. Melancon**[†], **Mei Tian**[†], **Dong Liang**[#], and **Chun Li**[†,*]

[†]Department of Experimental Diagnostic Imaging, The University of Texas MD Anderson Cancer Center, Houston, Texas 77030

[‡]On leave from the Department of Nuclear Medicine, Renji Hospital, Shanghai Jiaotong University, School of Medicine, Shanghai, P. R. China 200127

[#]Department of Pharmaceutical Sciences, Texas Southern University, Houston, TX 77004

Abstract

We synthesized and evaluated a novel class of chelator-free [^{64}Cu]-CuS nanoparticles (NPs) suitable for both PET imaging and as photothermal coupling agents for photothermal ablation. [^{64}Cu]-CuS NPs were simple to make, possessed excellent stability, and allowed robust noninvasive micro-PET imaging. Furthermore, CuS NPs displayed strong absorption in the near-infrared (NIR) region (peak 930 nm), passive targeting prefers the tumor site, and mediated ablation of U87 tumor cells upon exposure to NIR light both *in vitro* and *in vivo* after either intratumoral or intravenous injection. The combination of small diameter (~11 nm diameter), strong NIR absorption, and integration of ^{64}Cu as a structural component makes [^{64}Cu]-CuS NPs ideally suited for multifunctional molecular imaging and therapy.

Introduction

Positron emission tomography (PET) is a powerful and widely used diagnostic tool that has the advantages of high sensitivity (down to the picomolar level) and ability to provide quantitative imaging analyses of *in vivo* abnormalities.[1–3] ^{64}Cu ($T_{1/2}$ = 12.7 h; β^+, 0.653 MeV [17.8%]; β^-, 0.579 MeV [38.4%]) has decay characteristics that allow for both PET imaging and targeted radiotherapy for cancer.[4] It has been investigated as a promising radiotracer for real-time PET monitoring of regional drug concentration, pharmacokinetics, and dosimetry during radiotherapy.[4,5]

Radioisotopes have been introduced to various nanoparticles (NPs), including quantum dots,[6,7] gold NPs,[5,8,9] carbon nanomaterials,[10,11] and polymeric NPs,[12–15] through radionuclide labeling to allow noninvasive *in vivo* nuclear imaging of NPs' pharmacokinetics, tissue distribution, and clearance. In several studies, PET has been used to investigate the pharmacokinetics and biodistribution of ^{64}Cu-labeled NPs.[5,13] In all of

[*]To whom correspondence should be addressed: Chun Li, Department of Experimental Diagnostic Imaging-Unit 59, The University of Texas MD Anderson Cancer Center, 1515 Holcombe Boulevard, Houston, TX 77030. Phone: 713-792-5182; Fax: 713-794-5456; cli@mdanderson.org.

Supporting Information Available: Complete reference 31; Characterization data of CuS NPs: NMR, XRD, DLS; Stability, radiolabeling efficiency of CuS NPs; *In vitro* PTA therapy study. This material is avaible free of charge via the Internet at http://pubs.acs.org.

these studies, the radioisotopes are linked to NPs through chelators such as diethylene triamine pentaacetic acid or 1,4,7,10-tetraazacyclododecane-1,4,7,10-tetraacetic acid to form stable complexes.

However, there are two inherent limitations associated with the use of radiometal-chelator complexes for nuclear imaging and *in vivo* study of NPs.16 First, the physicochemical properties of NPs attached to radiometal-chelator complex are not exactly the same as those of NPs without radiotracers. It is well known that the biodistribution and pharmacokinetic properties of NPs are influenced by their surface properties.17 Therefore, the data obtained using NPs conjugated with radiometal-chelator complexes may not reflect the pharmacological properties of unlabeled NPs. Second, the radiometal-chelator complexes may be detached from the surface of the NPs, or the radiometal ions may be displaced *in vivo* from the radiometal-chelator complexes owing to transchelation in the presence of high plasma protein concentrations, which again could lead to *in vivo* data not accurately reflecting the pharmacokinetics and biodistribution of NPs.18 Therefore, it is necessary to validate the *in vivo* data acquired with chelator-based radiolabeling techniques with independent analytical tools.

Photothermal ablation (PTA) therapy has gained increasing attention in recent years as a minimally invasive alternative to conventional approaches to cancer treatment such as surgery and chemotherapy.19–22 NPs with unique optical properties—primarily gold nanostructures, such as gold nanoshells,23,24 gold nanorods,25,26 gold nanocages,27,28 and hollow gold nanospheres,5,8,29 but also carbon nanotubes30,31—have been investigated as photothermal coupling agents to enhance the efficacy of PTA therapy. These plasmonic nanomaterials exhibit strong absorption in the near-infrared (NIR) region (wavelength 700–1100 nm) and offer an opportunity to convert optical energy to thermal energy, enabling deposition of otherwise benign optical energy into tumors for thermal ablation of tumor cells.

As a well-known p-type semiconductor material, CuS is of great interest for use in catalysis and photovoltaic. Several methods have been developed for the preparation of copper sulfide nanoparticles.32–34 Semiconductor CuS NPs are a new class of promising photothermal coupling agents. In our previous work, we have synthesized thioglycolic acid-stabilized CuS NPs and demonstrated their application for photothermal destruction of tumor cells *in vitro* using a NIR laser beam centered at 808 nm.35 In the current study, we developed a process for the rapid synthesis of radioactive [^{64}Cu]-CuS NPs in which ^{64}Cu is an integral building block of CuS rather than chelated to NPs. Both citrate and polyethylene glycol (PEG)-stabilized [^{64}Cu]-CuS NPs were evaluated for their pharmacokinetic and biodistribution. We demonstrated *in vivo* passive targeting of the nanoparticles to tumors. We further investigated the photothermal killing effect of PEG-stabilized CuS NPs both *in vitro* and *in vivo* following intratumoral (i.t.) or intravenous (i.v.) injection. To the best of our knowledge, this is the first report on the use of chelator-free NPs for PET imaging and the first demonstration of CuS NPs for dual imaging and PTA therapy *in vivo*.

Experiment Section

Materials

Copper(II) chloride ($CuCl_2$), sodium sulfide ($Na_2S{\cdot}9H_2O$), sodium citrate, and methoxy–PEG–thiol (SH-PEG; molecular weight, 5,000) were purchased from Sigma-Aldrich (St. Louis, MO). Isoflurane was obtained from Baxter (Deerfield, IL). $^{64}CuCl_2$ was obtained from Wisconsin University at Madison (Madison, WI). PD-10 columns were purchased from Amersham-Pharmacia Biotech (Piscataway, NJ). All the chemicals and solvents were at least ACS grade and were used without further purification. Deionized water (18 MΩ)

was obtained from a Milli-Q synthesis system (Millipore, Billerica, MA). Human U87 glioblastoma cells were obtained from American Type Culture Collection (Manassas, VA). RPMI-1640 culture medium and calcein AM were obtained from Sigma-Aldrich.

Synthesis of CuS NPs

The general procedure for the synthesis of CuS NPs in water was as follows. Into 1000 mL of aqueous solution of $CuCl_2$ (0.1345 g, 1 mmol) and sodium citrate (0.2 g, 0.68 mmol) was added 1 mL of sodium sulfide solution (Na_2S, 1 M) under stirring at room temperature. The pale blue $CuCl_2$ solution turned dark brown immediately upon the addition of sodium sulfide. Five minutes later, the reaction mixture was heated to 90°C and stirred for 15 min until a dark green solution was obtained. The mixture was transferred to ice-cold water. The Cit-CuS NPs were obtained and stored at 4°C. To introduce PEG coating, about 1 mg of SH-PEG was added into the Cit-CuS NP solution (1.42×10^{15} NPs in 1.0 mL of water). The reaction was allowed to proceed overnight at room temperature.

Characterizations of CuS NPs

For transmission electron microscopy, aqueous solution of CuS NPs was deposited on carbon-enhanced copper grids without negative staining. The NPs were allowed to adhere on the grid for 1 h, after which they were briefly rinsed with deionized water and air dried. The samples were then examined using a transmission electron microscope (JEM 2010, JEOL Japan) at an accelerating voltage of 200 kV. Digital images were obtained using the AMT Imaging System (Advanced Microscopy Techniques Corp., Danvers, MA). The average diameter of CuS NPs was determined by measuring up to 200 individual particles. The UV-Vis spectroscopy of CuS NPs was recorded on a Beckman Coulter DU-800 UV-VIS spectrometer (Brea, CA) with a 1.0-cm optical path length quartz cuvette. The identity and crystallinity, crystalline structure, size, and shape of the NPs were observed by X-ray diffraction and a high-resolution transmission electron microscope (200 kV, JEOL, Japan). X-ray diffraction was performed using a Siemens Kristalloflex 810 D-500 X-ray diffractometer (Siemens, Germany) under an operating mode of 40 kV and 30 mA with λ = 1.5406 Angstrom radiation.

Stability of CuS NPs

The stability of Cit-CuS NPs and PEG-CuS NPs in various media was investigated by incubating CuS NPs in water, 0.4 mM citrate solution, 100 mM acetate buffer solution, 100 mM NaCl solution, 4-(2-hydroxyethyl)-1-piperazineethanesulfonic acid buffer, PBS, 50 mM bovine serum albumin solution, PBS containing 10% fetal bovine serum (FBS), or 100% FBS at 37°C for up to 7 days. The appearance of precipitation was observed by visual inspection.

Synthesis of radioactive [^{64}Cu]-CuS NPs

$^{64}CuCl_2$ (20 μL, 1000 μCi) was added to 1 mL of $CuCl_2$ solution (1 mM) containing sodium citrate (0.2 g/L). Then, 10 μL of sodium sulfide solution (100 mM) was added to the $CuCl_2$ solution under stirring. The mixture was then heated to 90°C for 15 min until a dark green solution was obtained. The reaction mixture was transferred to ice-cold water to give Cit-[^{64}Cu]-CuS NPs. The same procedure used for Cit-[^{64}Cu]-CuS NPs was used for the preparation of PEG-[^{64}Cu]-CuS NPs. Thus, 10 μL of sodium sulfide solution was added into 1 mL of aqueous solution of $^{64}CuCl_2/CuCl_2$ solution containing 1 mg of SH-PEG.

The radiolabeling efficiency and the stability of labeled NPs were analyzed using instant thin layer chromatography (ITLC). The ITLC strips were developed with PBS (pH 7.4) containing 4 mM ethylenediaminetetraacetic acid and quantified using a Bioscan IAR-2000

TLC Imaging Scanner (Washington, DC). For the study of labeling stability, Cit-[^{64}Cu]-CuS NPs and PEG-[^{64}Cu]-CuS NPs were suspended in PBS or mouse serum and incubated at 37°C for 24 h. Free $^{64}Cu^{2+}$ ions moved to the solvent front, and the NPs remained at the original spot. The radioactivity at the original spot was recorded as a percentage of the total radioactivity of the ITLC strip.

Pharmacokinetics

All experiments involving animals were done in accordance with the guidelines of the Institutional Animal Care and Use Committee. For pharmacokinetic analysis, mice were intravenously injected with radioactive CuS NPs (4×10^{11} particles, 50 μCi/mouse in 0.2 mL), and blood samples (10 μL) were collected from the tail vein at predetermined time points. The blood pharmacokinetic parameters of the radiotracer were analyzed with a two-compartmental model using WinNonlin 5.0.1 software (Pharsight Corporation, Palo Alto, CA). The animals were euthanized by CO_2 exposure at the end of the study.

Biodistribution-radioactivity counting

Human U87 glioblastoma tumors were grown subcutaneously in the right thigh of nude mice (20–25 g; Harlan-Sprague-Dawley, Indianapolis, IN) by injecting 1×10^6 viable tumor cells suspended in PBS. When tumors had grown to 5–8 mm in diameter, the mice were randomly allocated into two groups (n = 5). Mice in group 1 were injected with Cit-[^{64}Cu]-CuS NPs, and mice in group 2 were injected with PEG-[^{64}Cu]-CuS NPs, each at a dose of 8×10^{10} particles per mouse (20 μCi per mouse in 0.2 mL). Mice were killed by CO_2 overexposure 24 h after injection. Blood, heart, liver, spleen, kidney, lung, stomach, intestine, muscle, bone, brain, and tumor tissues were removed and weighed, and radioactivity was measured with a Packard Cobra gamma counter (Ramsey, MN). Uptakes of ^{64}Cu-labeled CuS NPs in various organs were expressed as percentage of injected dose per gram of tissue (%ID/g).

*micro*PET/CT imaging

Mice bearing U87 tumors were prepared as before. When tumors reached 8–10 mm in diameter, mice (n = 3) were treated with an i.v. injection of PEG-[^{64}Cu]-CuS NPs (8×10^{10} particles/mouse, 200 μCi/mouse; 0.2 mL). The animals were anesthetized with 2% isoflurane and placed in prone position, and micro-PET/CT images were acquired at 1, 6, and 24 h after injection of radiolabeled nanoparticles using an Inveon micro-PET/CT scanner (Siemens Preclinical Solution, Knoxville, TN). The micro-PET and CT images were generated separately and then fused using Inveon Research Workplace (Siemens Preclinical Solution, Knoxville, TN). For data analysis, the region of interest (ROI) was manually drawn covering the whole tumor on CT and copied to the corresponding PET images. Similarly, a circular region of interest was drawn on the muscle of the opposite leg of the mouse on CT images, and copied to the PET images. The mean signal intensities of the tumor and muscle in the ROIs were recorded. The tumor-to-muscle ratio was calculated by dividing signal intensity of the tumor by that of the muscle.

Photothermal effect in aqueous solution

The laser was a continuous-wave GCSLX-05–1600m-1 fiber-coupled diode laser with a center wavelength of 808 ± 10 nm. It was powered by a DH 1715A-5 dual-regulated power supply (15PLUS laser, Diomed, Andover, MA). A 5-m, 600-μm core BioTex LCM-001 optical fiber (BioTex Inc., Houston, TX) was used to transfer laser power from the laser unit to the target. This fiber had a lens mounting at the output that allowed the laser spot size to be changed by changing the distance from the output to the target. The output power was independently calibrated using a handheld model 840-C optical power meter (Newport Corporation, Irvine, CA) and was found to be 1 W for a spot diameter of 3.5 mm (~8 W/

cm^2) and a 2-amp supply current. The end of the optical fiber was attached to a retort stand using a movable clamp and positioned directly above the sample cell. For measuring temperature change mediated by CuS NPs, NIR laser light (808 nm) was delivered through a quartz cuvette containing the CuS NPs (100 μL). A thermocouple was inserted into the solution perpendicular to the path of the laser light. The temperature was measured over 10 min. Water was used as a control.

Photothermal ablation of cancer cells with CuS NPs *in vitro*

U87 cells were seeded onto a 96-well plate with a density of 10,000 per well 1 day before the experiment. Cells were washed three times with Hanks balanced salt solution (HBSS, Sigma-Aldrich) and then incubated with PEG-CuS NPs in RPMI-1640 culture medium (Invitrogen, Carlsbad, CA) at CuS concentrations of 100 μM or 500 μM at 37°C. Cells without NPs were used as a control. Two hours later, the culture medium was replaced with fresh RPMI-1640 medium without phenol red, and the cells were irradiated with a diode NIR laser centered at 808 nm at an output power of 0, 16 W/cm^2 for 5 min, 40 W/cm^2 for 5 min, or 40 W/cm^2 for 2 min. The laser was coupled to a 1-m, 2-mm core fiber, which delivered a circular laser beam of 4 mm in diameter, covering the central area of the microplate well. Power calibration was done automatically. After treatment, cells were resupplied with RPMI-1640 containing 10% FBS. Twenty-four h later, the cells were washed with HBSS and stained with calcein AM for visualization of viable cells according to manufacturer's suggested protocol (Invitrogen). Cells were examined under a Zeiss Axio Observer.Z1 fluorescence microscope (Carl Zeiss MicroImaging GmbH, Göttingen, Germany).

Photothermal ablation of cancer cells with CuS NPs *in vivo*

Nude mice were inoculated subcutaneously with 5×10^6 U87 cells in the right side of the rear leg 21 days before the experiment. When tumor had grown to 7–10 mm in diameter, mice were randomly allocated into 5 groups (n = 5). Mice in group A were injected intratumorally with PEG-CuS NPs (5 μL, 8 mM/mouse, 4×10^{13} NPs/mouse). Mice in groups B and C were injected intravenously with PEG-CuS NPs (200 μL, 8 mM/mouse). Mice in group D were injected intravenously with saline. Mice in group E did not receive any treatment. After 24 h, the tumors in mice from groups A, B, and D were irradiated with NIR laser at 12 W/cm^2 for 5 min. The mice were killed 24 h after laser treatment, and tumors were removed, snap frozen, and cryosectioned into 1000 μm. The slides were stained with hematoxylin-eosin. The slices were examined under a Zeiss Axio Observer.Z1 fluorescence microscope. The images were taken using a Zeiss AxioCam MRc5 color camera, and the extent of tumor necrosis, expressed as a percentage of the entire tumor area, was analyzed with Zeiss AxioVision software (version 4.6.3).

Statistical analysis

Differences in biodistribution data and extent of necrosis expressed as percentage of necrotic area after treatments were analyzed using two-tailed Student's *t* test. Differences between groups were considered statistically significant at $p < 0.05$.

Results and Discussion

Synthesis, characterization, and stability

Citrate-coated CuS NPs (Cit-CuS NPs) were readily synthesized in aqueous solution by reacting $CuCl_2$ and Na_2S in the presence of sodium citrate at 90°C for 15 min. PEG coating was introduced by incubating Cit-CuS NPs with SH-PEG (molecular mass, 5,000 Da) at room temperature overnight. The coating of citrate and PEG to the surface of CuS NPs were

confirmed using nuclear magnetic resonance analysis (Supporting Information, Figure S1). All X-ray diffraction peaks of the CuS NPs (Supporting Information, Figure S2) could be indexed as covellite-phase CuS with lattice parameters similar to those of the Joint Committee on Powder Diffraction Standards card 79–2321. The diffraction peaks were relatively broad, reflecting the small size of CuS crystals. No obvious impurity peaks were detected, indicating the acquirement of covellite CuS with high quality. Figure 1A is a representative transmission electron microscopy image of the CuS NPs. The CuS NPs were well dispersed and relatively uniform in size, with an average diameter of 11 nm. The hydrodynamic sizes of the CuS NPs were determined from dynamic light scatting study (Supporting Information Figure S3). CuS NPs which had a TEM diameter of 11 nm showed DLS size of 11.7 nm and 31.6 nm before and after PEG coating, respectively. The increased diameter of PEG-coated NPs in aqueous solution is probably due to the PEG layer that is invisible in TEM measurement. These CuS NPs were significantly larger than previously reported thioglycolic acid-stabilized CuS NPs, which had an average diameter of 3 nm and displayed peak absorbance at 900 nm.35 The high-resolution TEM (Supporting Information Figure S4) reveals the fringes of hexagonal CuS (102) planes with a lattice spacing of about 0.3 nm. These results are in agreement with the lattice spacing of the {102} plane (0.305 nm) of hexagonal CuS nanostructures described in previous reports.36,37 The optical spectra of Cit-CuS NPs and PEG-CuS NPs are shown in Figure 1B. Both types of NPs displayed a blue-shifted band gap absorption compared to bulk CuS materials (peak >1100 nm),38 confirming the effect of quantum size confinement. On the basis of the measured absorbance *A*, the extinction coefficient was calculated to be about $8.66 \times 10^7\ M^{-1}cm^{-1}$ at the peak absorption of 930 nm using the following equation:

$$\varepsilon=(A\pi/6d^3\rho N_A)/(LC_{wt})$$

where *d* is the average diameter of the CuS NPs assuming the NPs are spherical, ρ is the density of the NPs assuming it is the same as the bulk (~4.6 g/cm^3), N_A is Avogadro's constant, L is the path length (1 cm), and C_{wt} is the weight concentration of the NPs.

These are typical characteristics of covellite CuS and can be interpreted in terms of valence-band-free carriers (positive holes), which are essentially metallic in character and give rise to NIR plasmon absorption because of high charge density.38 On the basis of X-ray diffraction, UV-vis spectroscopy, and transmission electron microscopy results, we concluded that we had made pure and high-quality CuS NPs. It is worth noting that the maximum absorption of the 11-nm Cit-CuS NPs and PEG-CuS NPs, 930 nm, is 30 nm red-shifted compared to the absorption of the 3-nm CuS NPs previously reported by our groups35 but is 50 nm blue-shifted compared to the absorption of the 15-nm CuS NPs previously reported by Zhao et al,38 who studied the composition dependence of plasmonic resonance spectra of $Cu_{2-x}S$. Future studies are needed to identify and clarify the effect of size on the NIR plasmonic resonance spectra for CuS NPs.

The stability of Cit-CuS NPs and PEG-CuS NPs was investigated by incubating these NPs in various media, including water, 0.4 mM citrate solution, 100 mM acetate buffer solution, 100 mM NaCl solution, 4-(2-hydroxyethyl)-1-piperazineethanesulfonic acid buffer (HEPES), phosphate-buffered saline (PBS), 50 mM bovine serum albumin solution, PBS containing 10% fetal bovine serum (FBS), and 100% FBS at 37°C for up to 7 days. No precipitates were observed and no obvious change of hydrodynamic particle sizes were found for either type of NP in these solutions (Supporting Information, Figure S5 and Table S1), indicating that both Cit-CuS NPs and PEG-CuS NPs possess excellent colloidal stability under a wide range of environmental conditions.

[^{64}Cu]-CuS NPs were prepared using the same procedures used for the preparation of plain CuS NPs except that for the synthesis of PEG-[^{64}Cu]-CuS NPs, the PEG coating was introduced directly during the course of CuS NP synthesis instead of after CuS NP formation through PEG/citrate substitution. This is necessary to shorten the time of synthesis for [^{64}Cu]-CuS NPs. The preparation of the 3-nm CuS described in a previously reported procedure requires more than 24 h for the reaction to complete at room temperature, which is not suitable for ^{64}Cu labeling because the decay half-life of ^{64}Cu is only 12.7 h. High reaction temperature was used for rapid radio-synthesis of PEG-[^{64}Cu]-CuS NPs, reducing the time of PEG-[^{64}Cu]-CuS NP production to ~20 min. The specific activity was readily controlled by varying the radioactivity of $^{64}CuCl_2$ in the mixture of $^{64}CuCl_2$ and cold $CuCl_2$ at the time of [^{64}Cu]-CuS synthesis. As shown in Table 1, 100% of radioactivity was associated with Cit-[^{64}Cu]-CuS NPs and PEG-[^{64}Cu]-CuS NPs at the end of synthesis, indicating that the radiolabeling efficiency approached 100%. After incubation in PBS and FBS at 37°C for 24 h, Cit-[^{64}Cu]-CuS NPs lost 12.7% and 15.3% of radioactivity, respectively. However, negligible amount of radioactivity was lost from PEG-[^{64}Cu]-CuS NPs. These data indicated that ^{64}Cu was more stably integrated in PEG-[^{64}Cu]-CuS NPs than in Cit-[^{64}Cu]-CuS NPs (Table 1 and Supporting Information, Figure S6).

Pharmacokinetics, biodistribution, and PET Imaging

Blood activity–time profiles of Cit-[^{64}Cu]-CuS NPs and PEG-[^{64}Cu]-CuS NPs are shown in Figure 2A and their pharmacokinetic parameters are presented in Table 2. Both formulations appeared to have very different *in vivo* disposition characteristics. The mean systemic clearance was significantly slower with PEG (0.48 mL/h) than with citrate (0.75 mL/h, $p = 0.003$), suggesting that citrate-coated CuS NPs were cleared faster than PEG-coated NPs following intravenous administration. This may be attributed to higher uptake by reticuloendothelial systems (RES), i.e., liver and spleen, and consequently faster elimination of Cit-[^{64}Cu]-CuS NPs than that of PEG-[^{64}Cu]-CuS NPs. As a result, PEG-[^{64}Cu]-CuS NPs had a significantly higher systemic exposure, i.e., area under the curve (AUC = 213.7 %ID h/mL), than that of Cit-[^{64}Cu]-CuS NPs (134.9 %ID h/mL, $p = 0.008$). The mean volume of distribution at steady-state was higher with citrate coated NPs (5.8 mL) than with PEG coated NPs (3.79 mL, $p = 0.018$), suggesting that citrate coated NPs has higher uptake in such tissues as liver and spleen. Interestingly, there was no difference between the two CuS NP formulations in the half-lives ($t_{1/2\alpha} = 0.76$ h and $t_{1/2\beta} = 5.98$ for Cit-[^{64}Cu]-CuS NPs versus $t_{1/2\alpha} = 0.71$ h and $t_{1/2\beta} = 6.06$ h for PEG-[^{64}Cu]-CuS NPs). This was likely due to the compensatory effect of systemic clearance and the volume of distribution. For each formulation, volume of distribution at steady-state was close to the volume of distribution in the central compartment, indicating that the drug mainly distributed to the central compartment (systemic blood circulation).

Biodistribution data obtained 24 h after i.v. injection of Cit-[^{64}Cu]-CuS NPs and PEG-[^{64}Cu]-CuS NPs are shown in Figure 2B. Cit-[^{64}Cu]-CuS NPs displayed significantly higher uptake than did PEG-[^{64}Cu]-CuS NPs in the liver and the spleen, both are RES enriched tissues. Conversely, PEG-[^{64}Cu]-CuS NPs were less likely being captured by RES cells, and therefore, displayed higher levels in the heart, kidney, lung, stomach, intestine, and bone. These findings are consistent with the pharmacokinetic findings that PEG-[^{64}Cu]-CuS NPs has a slower systemic clearance than that of Cit-[^{64}Cu]-CuS NPs, which made it more available to distribute to target tissues. Importantly, uptake in human U87 glioblastoma xenografts in mice was almost 3 times as high with PEG-[^{64}Cu]-CuS NPs as with Cit-[^{64}Cu]-CuS NPs at 24 hr after i.v. injection (7.6 ±1.4 %ID/g vs. 2.6 ± 0.4 %ID/g, $p = 0.011$). This may be attributed to the enhanced permeability and retention effect of NPs, and greater systemic exposure of PEG-[^{64}Cu]-CuS NPs, which made it more available to the tumor uptake. This effect can be utilized for passive targeting of NPs to areas with increased

angiogenesis, where NPs with longer blood circulation time exhibit higher tumor uptake.[9,15]

Because they had greater radiolabel stability and a higher tumor uptake value than Cit-[^{64}Cu]-CuS NPs, PEG-[^{64}Cu]-CuS NPs were further evaluated with regard to their utility for *in vivo* PET. Figure 3 shows representative whole-body micro-PET/CT images of a mouse acquired at 1, 6, and 24 h after i.v. injection of PEG-[^{64}Cu]-CuS NPs. Consistent with the biodistribution analysis, PET/CT images revealed high uptake of PEG-[^{64}Cu]-CuS NPs in the liver and the spleen. As expected, PEG-[^{64}Cu]-CuS NPs gradually accumulated in the tumor between 1 h and 24 h, permitting remarkably clear visualization of the tumor at 24 h after injection. Quantitative analysis showed that the average tumor-to-muscle ratios at 1 h, 6 h, and 24 h after NP injection were 2.74:1, 6.14:1, and 6.55:1, respectively, indicating that PEG-[^{64}Cu]-CuS NPs were deposited in and retained in the tumor over the 24-h period. These values compared favorably with those for ^{64}Cu-labeled quantum dots targeted to integrin $\alpha_v\beta_3$ receptors, where RGD-coated quantum dots were found to have a tumor-to-muscle ratio of 4:1 at 5 h after i.v. injection into nude mice with U87 tumors.7 PEG-[^{64}Cu]-CuS NPs were excreted by both renal and hepatobiliary routes, as indicated by the deposition of radioactivity in the bladder and the gastrointestinal tract (Fig. 3). Instant thin-layer chromatography study revealed that PEG-[^{64}Cu]-CuS NPs were cleared from the renal system in the form of nanoparticles (Supporting Information, Figure S7). A previous study by Choi et al. 39 with quantum dots demonstrated that NPs smaller than 5 nm can be cleared by the renal route. Although the average diameter of the CuS NPs was 11 nm, it is possible that a small fraction of the CuS NPs smaller than 5 nm in diameter were capable of renal clearance.

In vitro and *in vivo* photothermal therapy

To date, there have been few reports on NPs smaller than 20 nm having NIR absorption.35 The smallest gold nanostructures reported to date as having plasmon NIR absorption were ~40 nm in diameter.[8,29] Because the pharmacokinetics and biodistribution pattern of NPs are strongly affected by their size,[9,15] it is highly desirable that novel nanostructures having diameter less than 20 nm with NIR absorption be identified and evaluated. CuS NPs, which are much smaller than gold nanostructures, may have a better chance of reaching their targets and being cleared from the body through the renal system.[9,39,40]

An important feature of CuS NPs is NIR light-induced thermal effect, which could be used for PTA therapy. To investigate temperature elevation induced by NIR laser irradiation in the presence of CuS NPs, we used a continuous-wave fiber-coupled diode laser centered at 808 nm. Figure 4A shows the temperature change of an aqueous solution containing PEG-CuS NPs as a function of exposure time. Exposure of an aqueous solution of PEG-CuS NPs (500 μM CuS molecular units, 7.1×10^{14}/mL [23 nM CuS NP]) to the NIR laser light (16 W/cm^2) for 5 min elevated the temperature of the solution from 25°C to 80°C (an increase of 55°C). Under the same conditions, no change in temperature was observed with pure water. The magnitude of increase in temperature of the aqueous solution of PEG-CuS NPs decreased with decreasing PEG-CuS NP concentration (Fig. 4B). These data indicated that PEG-CuS NPs acted as an efficient photothermal coupling agent. Compared with our previously reported 3-nm CuS NPs,35 the new 11-nm CuS NPs displayed higher photothermal conversion efficiency. For example, the temperature of an aqueous solution of 3-nm CuS NPs increased 12.7°C over a period of 5 min at an output power of 24 W/cm^2 and a concentration of 770 μM CuS units (~4.8×10^{16} particles/mL).35

To test the cell killing induced by photothermal effect through CuS NPs, human U87 glioblastoma cells were incubated with PEG-CuS NPs for 2 h. The cells were then irradiated with NIR laser centered at 808 nm. The cell viability after exposure to NIR laser was probed

using calcein AM dye, which reports ubiquitous intracellular esterase activity. Twenty-four hours after laser treatment, cells treated with PEG-CuS NPs at a concentration of 500 μM CuS plus NIR laser (16 W/cm^2 for 5 min, 40 W/cm^2 for 2 min, or 40 W/cm^2 for 5 min) had substantially reduced cell density (Supporting Information, Figure S8). No apparent change in cell viability was observed when cells were treated with CuS NPs alone at 100 μM or 500 μM or NIR laser alone at 16 W/cm^2 for 5 min or 40 W/cm^2 for 5 min. These results indicated that PEG-CuS NPs mediated photothermal destruction of U87 cells.

In mice bearing subcutaneous U87 tumors, the skin of the mice at the tumor site turned greenish after both i.t. and i.v. injection of PEG-CuS NPs owing to the deposition of the NPs in the tumor (Fig. 5A). After NIR irradiation, the skin at the tumor sites in both mice that received i.t. injection and mice that received i.v. injection of PEG-CuS NPs turned brownish or dark red, indicating tissue burn caused by local photothermal effect. In contrast, there was no noticeable change in the skin of mice treated with PEG-CuS NPs alone, saline plus NIR irradiation, or NIR laser alone (Fig. 5A).

Histological examination confirmed that the combination of PEG-CuS NPs administered by either i.t. or i.v. injection followed by laser treatment caused significantly greater necrotic response than did PEG-CuS NPs without laser, saline plus laser, or saline only (Fig. 5B). In the mice treated with PEG-CuS NPs plus laser, common features of thermonecrosis, such as loss of nucleus, cell shrinkage, and coagulation, were found in the tumor tissues. In the mice treated with i.t. injection of PEG-CuS NPs plus laser, almost all of the tumor tissue was necrotized, exhibiting pyknosis, karyolysis, cytoplasmic acidophilia, and degradation and corruption of the extracellular matrix of the tumor. In the mice treated with i.v. injection of PEG-CuS NPs plus laser, about 65% of the tumor tissue was necrotized. In the mice treated with saline plus laser, there was only a baseline fraction of necrosis in tumor tissue (<5%). In the tumors of mice treated with CuS NPs alone (i.t. injection), saline plus NIR laser, or saline alone, there was little pyknosis or karyolysis, confirming the benign nature of these treatments (Fig. 5C). Thus, selective *in vivo* photothermal destruction of the tumors mediated by PEG-CuS NPs was confirmed.

Conclusions

In summary, PEG-[^{64}Cu]-CuS NPs acted as an efficient radiotracer for pharmacokinetics, biodistribution, and PET imaging, and PEG-CuS NPs acted as an efficient photothermal coupling agent. The combination of small size, strong absorption in the NIR region, and integration of positron emitter ^{64}Cu into the core structural component makes [^{64}Cu]-CuS NPs ideally suited for theranostic applications, i.e., image-guided PTA therapy. PEG-[^{64}Cu]-CuS NPs showed high uptake in U87 human glioblastoma xenografts owing to enhanced permeability and retention effect. Future studies will focus on active targeting of [^{64}Cu]-CuS NPs to solid tumors by conjugating receptor-specific targeting moieties onto the NPs' surface. Improved tumor uptake of PEG-[^{64}Cu]-CuS NPs should increase the efficacy of photothermal ablation therapy, decrease the energy dose of the laser, and minimize the potential damage to surrounding normal tissues. In addition to serving as a photothermal mediator, [^{64}Cu] and potentially [^{67}Cu]-labeled CuS NPs may also have an application for radiotherapy. Thus, the multifunctional [^{64}Cu]-CuS NPs combining intrinsic nuclear and optical properties for PET imaging and photothermal therapy represent a new nanoplatform for theranostic applications.

Supplementary Material

Refer to Web version on PubMed Central for supplementary material.

Acknowledgments

We thank Stephanie Deming for editing the article and Qian Huang and Meng Zhong for helping with animal and cell culture studies. We also thank Professor Wei Chen (The University of Texas at Arlington) for helpful discussion. This work was supported in part by National Institutes of Health Cancer Center Support Grant CA016672, National Institutes of Health grant R01 CA119387, a seed grant through the Alliance for NanoHealth by the U.S. Department of Army Telemedicine and Advanced Technology Research Center (W81XWH-07-2-0101), the John S. Dunn Research Foundation, and Shanghai Leading Academic Discipline Projects, China (S30203) (to SS).

References

1. Scheinin H, Scheinin M, Knuuti J. Ann. Med. 1999; 31:430–431. [PubMed: 10680857]
2. Eckelman WC. Drug Discov. Today. 2003; 8:404–410. [PubMed: 12706658]
3. Welch MJ, Hawker CJ, Wooley KL. J. Nucl. Med. 2009; 50:1743–1746. [PubMed: 19837751]
4. Shokeen M, Anderson CJ. Acc. Chem. Res. 2009; 42:832–841. [PubMed: 19530674]
5. Lu W, Zhang G, Zhang R, Flores LG 2nd, Huang Q, Gelovani JG, Li C. Cancer Res. 2010; 70:3177–3188. [PubMed: 20388791]
6. Schipper ML, Cheng Z, Lee SW, Bentolila LA, Iyer G, Rao JH, Chen XY, Wul AM, Weiss S, Gambhirl SS. J. Nucl. Med. 2007; 48:1511–1518. [PubMed: 17704240]
7. Cai W, Chen K, Li ZB, Gambhir SS, Chen X. J. Nucl. Med. 2007; 48:1862–1870. [PubMed: 17942800]
8. Melancon MP, Lu W, Yang Z, Zhang R, Cheng Z, Elliot AM, Stafford J, Olson T, Zhang JZ, Li C. Mol. Cancer Ther. 2008; 7:1730–1739. [PubMed: 18566244]
9. Zhang G, Yang Z, Lu W, Zhang R, Huang Q, Tian M, Li L, Liang D, Li C. Biomaterials. 2009; 30:1928–1936. [PubMed: 19131103]
10. McDevitt MR, Chattopadhyay D, Jaggi JS, Finn RD, Zanzonico PB, Villa C, Rey D, Mendenhall J, Batt CA, Njardarson JT, Scheinberg DA. Plos One. 2007; 2:1–10.
11. Liu Z, Cai WB, He LN, Nakayama N, Chen K, Sun XM, Chen XY, Dai HJ. Nat. Nanotechnol. 2007; 2:47–52. [PubMed: 18654207]
12. Pressly ED, Rossin R, Hagooly A, Fukukawa KI, Messmore BW, Welch MJ, Wooley KL, Lamm MS, Hule RA, Pochan DJ, Hawker CJ. Biomacromolecules. 2007; 8:3126–3134. [PubMed: 17880180]
13. Schluep T, Hwang J, Hildebrandt IJ, Czernin J, Choi CHJ, Alabi CA, Mack BC, Davis ME. Proc. Natl. Acad. Sci. U. S. A. 2009; 106:11394–11399. [PubMed: 19564622]
14. Yang Z, Zheng S, Harrison WJ, Harder J, Wen X, Gelovani JG, Qiao A, Li C. Biomacromolecules. 2007; 8:3422–3428. [PubMed: 17958440]
15. Yang Z, Leon J, Martin M, Harder JW, Zhang R, Liang D, Lu W, Tian M, Gelovani JG, Qiao A, Li C. Nanotechnology. 2009; 20:165101–165108. [PubMed: 19420561]
16. Sanhai WR, Sakamoto JH, Canady R, Ferrari M. Nat. Nanotech. 2008; 3:242–244.
17. Schipper ML, Iyer G, Koh AL, Cheng Z, Ebenstein Y, Aharoni A, Keren S, Bentolila LA, Li JQ, Rao JH, Chen XY, Banin U, Wu AM, Sinclair R, Weiss S, Gambhir SS. Small. 2009; 5:126–134. [PubMed: 19051182]
18. Bass LA, Wang M, Welch MJ, Anderson CJ. Bioconjugate Chem. 2000; 11:527–532.
19. Amin Z, Donald JJ, Masters A, Kant R, Steger AC, Bown SG, Lees WR. Radiology. 1993; 187:339–347. [PubMed: 8475270]
20. Nolsoe CP, Torppedersen S, Burcharth F, Horn T, Pedersen S, Christensen NEH, Olldag ES, Andersen PH, Karstrup S, Lorentzen T, Holm HH. Radiology. 1993; 187:333–337. [PubMed: 8475269]
21. Fiedler VU, Schwarzmaier HJ, Eickmeyer F, Muller FP, Schoepp C, Verreet PR. J. Magn. Reson. Imaging. 2001; 13:729–737. [PubMed: 11329194]
22. Vogel A, Venugopalan V. Chem. Rev. 2003; 103:577–644. [PubMed: 12580643]
23. Hirsch LR, Stafford RJ, Bankson JA, Sershen SR, Rivera B, Price RE, Hazle JD, Halas NJ, West JL. Proc. Natl. Acad. Sci. U. S. A. 2003; 100:13549–13554. [PubMed: 14597719]

24. Loo C, Lowery A, Halas N, West J, Drezek R. Nano Lett. 2005; 5:709–711. [PubMed: 15826113]
25. Dickerson EB, Dreaden EC, Huang XH, El-Sayed IH, Chu HH, Pushpanketh S, McDonald JF, El-Sayed MA. Cancer Lett. 2008; 269:57–66. [PubMed: 18541363]
26. Park JH, von Maltzahn G, Xu MJ, Fogal V, Kotamraju VR, Ruoslahti E, Bhatia SN, Sailor MJ. Proc. Natl. Acad. Sci. U. S. A. 2010; 107:981–986. [PubMed: 20080556]
27. Chen JY, Wang DL, Xi JF, Au L, Siekkinen A, Warsen A, Li ZY, Zhang H, Xia YN, Li XD. Nano Lett. 2007; 7:1318–1322. [PubMed: 17430005]
28. Au L, Zheng DS, Zhou F, Li ZY, Li XD, Xia YN. Acs Nano. 2008; 2:1645–1652. [PubMed: 19206368]
29. Lu W, Xiong C, Zhang G, Huang Q, Zhang R, Zhang JZ, Li C. Clin. Cancer Res. 2009; 15:876–886. [PubMed: 19188158]
30. Chakravarty P, Marches R, Zimmerman NS, Swafford ADE, Bajaj P, Musselman IH, Pantano P, Draper RK, Vitetta ES. Proc. Natl. Acad. Sci. U. S. A. 2008; 105:8697–8702. [PubMed: 18559847]
31. Burke A, et al. Proc. Natl. Acad. Sci. U. S. A. 2009; 106:12897–12902. [PubMed: 19620717]
32. Haram SK, Mahadeshwar AR, Dixit SG. J. Phys. Chem. 1996; 100:5868–5873.
33. Xu LM, Chen X, Ma L, Gao FQ. Colloid Surf. A. 2009; 349:69–73.
34. Huang P, Li ZM, Hu HY, Cui DX. J. Nanomater. 2010; 2010:1–6.
35. Li YB, Lu W, Huang Q, Huang M, Chen W, Li C. Nanomed. in press.
36. Wu CY, Yu S-H, Chen SF, Liu GN, Liu BH. J. Mater. Chem. 2006; 16:3326–3331.
37. Xu HL, Wang WZ, Zhu W. Mat. Lett. 2006; 60:2203–2206.
38. Zhao Y, Pan H, Lou Y, Qiu X, Zhu J, Burda C. J. Am. Chem. Soc. 2009; 131:4253–4261. [PubMed: 19267472]
39. Choi HS, Liu W, Misra P, Tanaka E, Zimmer JP, Itty Ipe B, Bawendi MG, Frangioni JV. Nat. Biotechnol. 2007; 25:1165–1170. [PubMed: 17891134]
40. Burns AA, Vider J, Ow H, Herz E, Penate-Medina O, Baumgart M, Larson SM, Wiesner U, Bradbury M. Nano Lett. 2009; 9:442–448. [PubMed: 19099455]

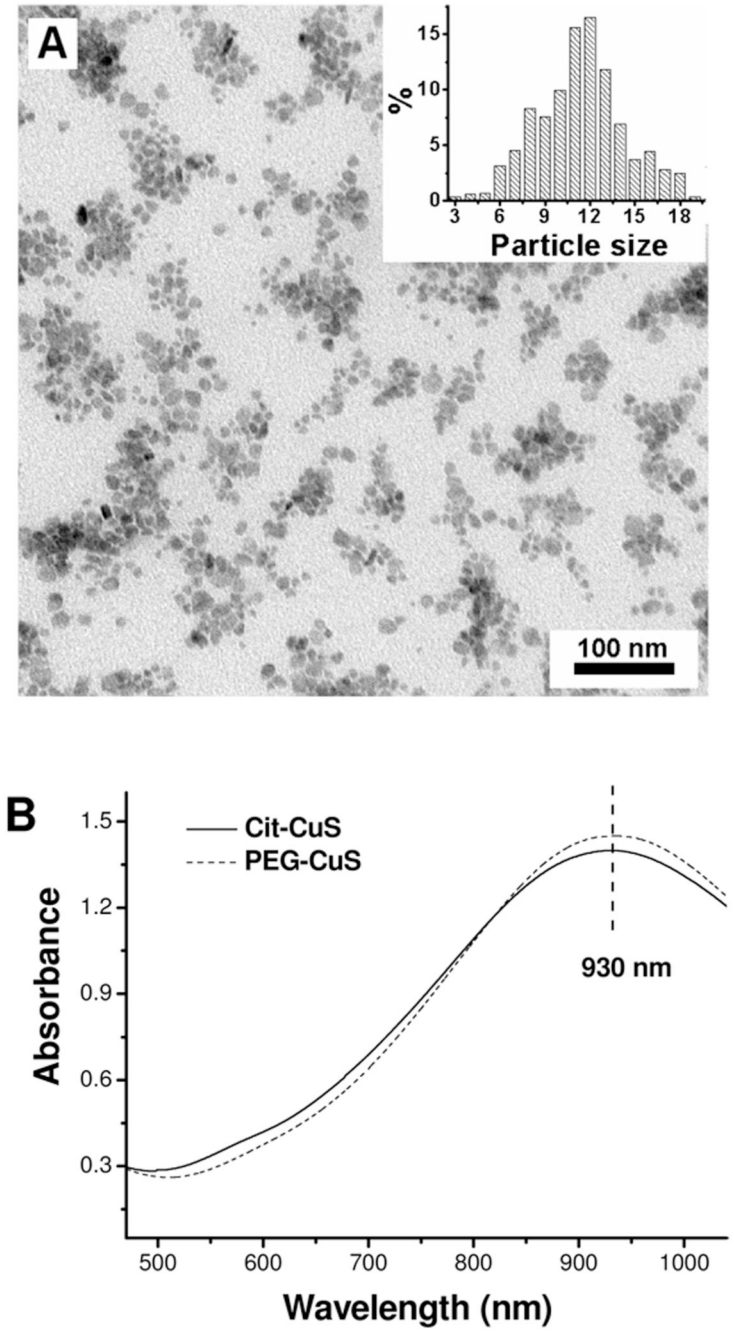

Figure 1.
Characterization of CuS NPs. (A) TEM image of PEG-CuS NPs. Inset: particle size distribution. (B) Absorption spectra of Cit-CuS NPs and PEG-CuS NPs.

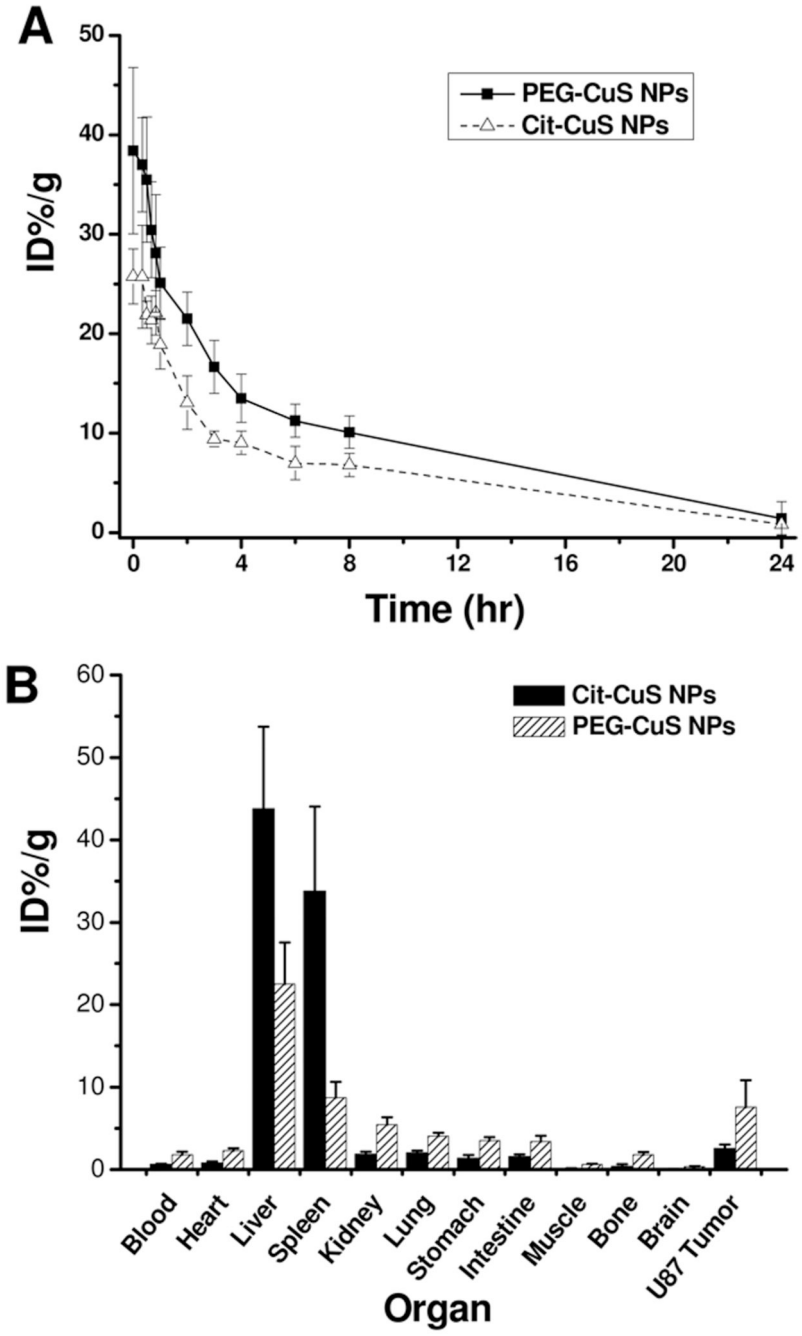

Figure 2.

Pharmacokinetic profiles of Cit-CuS NPs (n = 3) and PEG-CuS NPs (n = 5) following intravenous administration in mice (A); and biodistribution (B) of Cit-CuS NPs (n = 5) and PEG-CuS NPs (n = 5) at 24 h after intravenous injection in mice bearing subcutaneous U87 glioma xenografts. Data represent mean ± standard deviation.

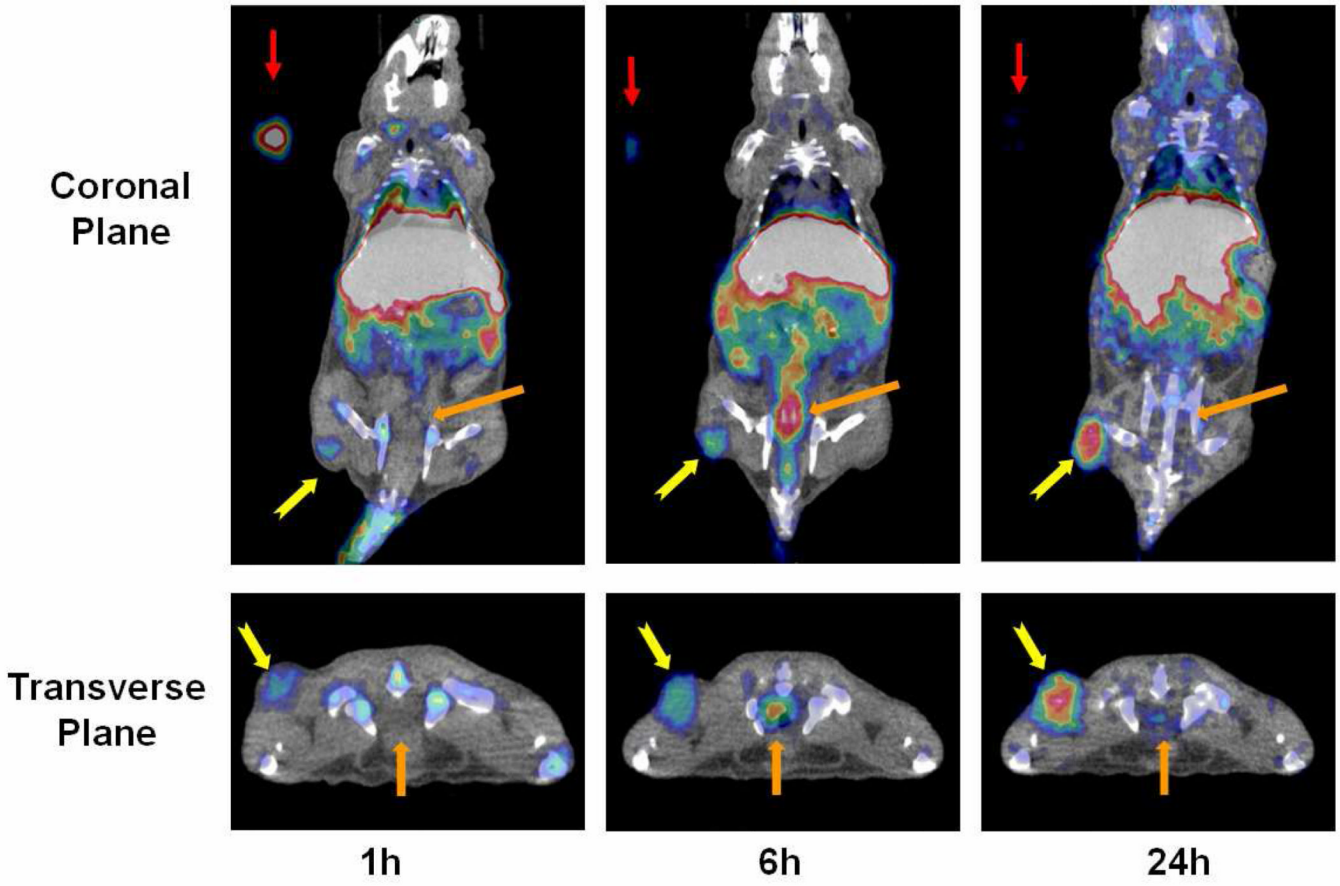

Figure 3.
Micro-PET/CT images of nude mice-bearing s.c. U87 glioma xenografts acquired at 1, 6, and 24 h after i.v. injection of PEG-[^{64}Cu]-CuS NPs. Yellow arrow: tumor; orange arrow: bladder; Red arrow: standard.

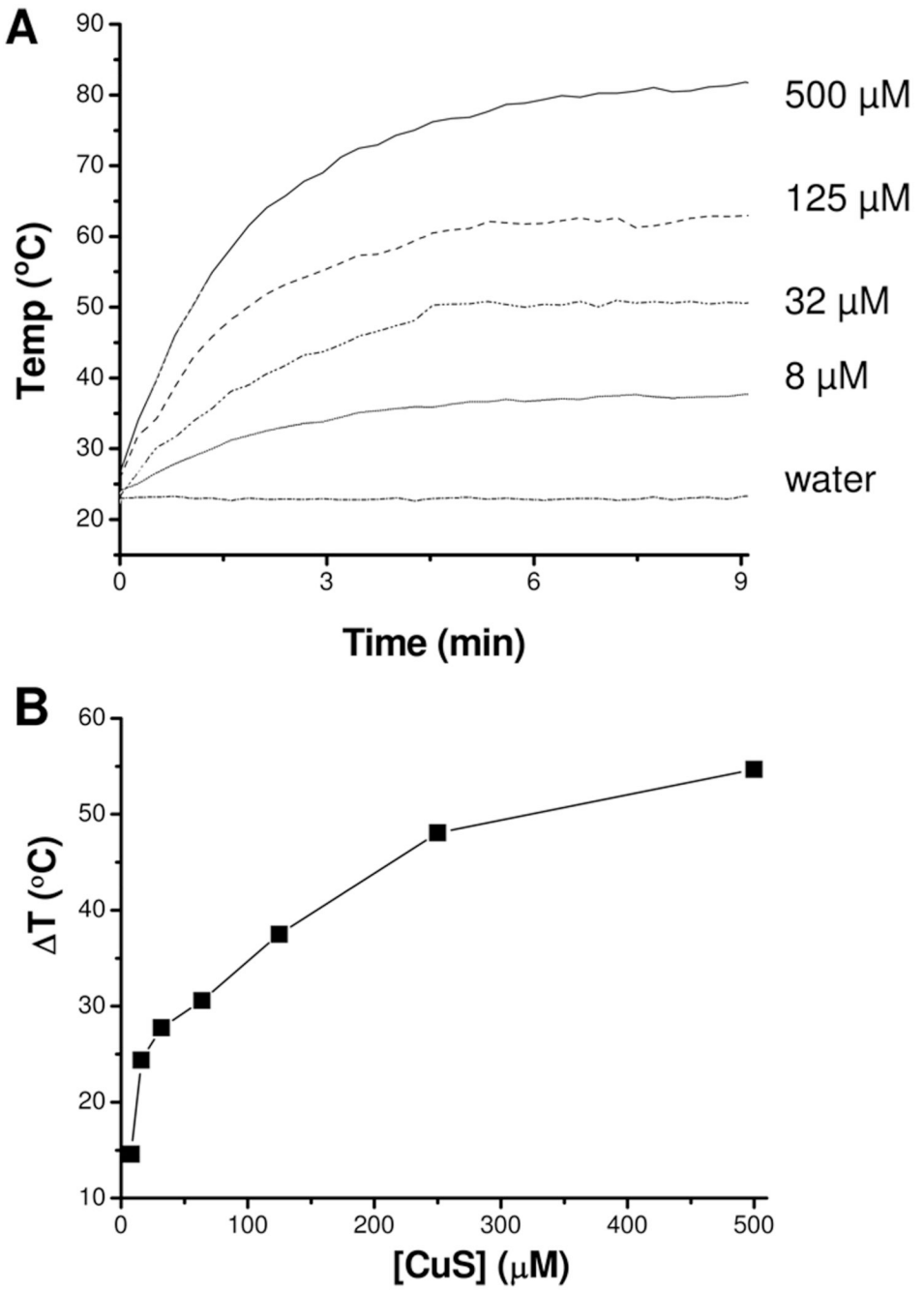

Figure 4.

PEG-CuS NPs acted as an efficient photothermal coupling agent. (A) Temperature elevation over a period of 9 min of exposure to NIR light (16 W/cm^2) at various PEG-CuS NP concentrations. Water was used as control. (B) Temperature change (ΔT) over a period of 9 min as a function of PEG-CuS NP concentration expressed as CuS molecular units.

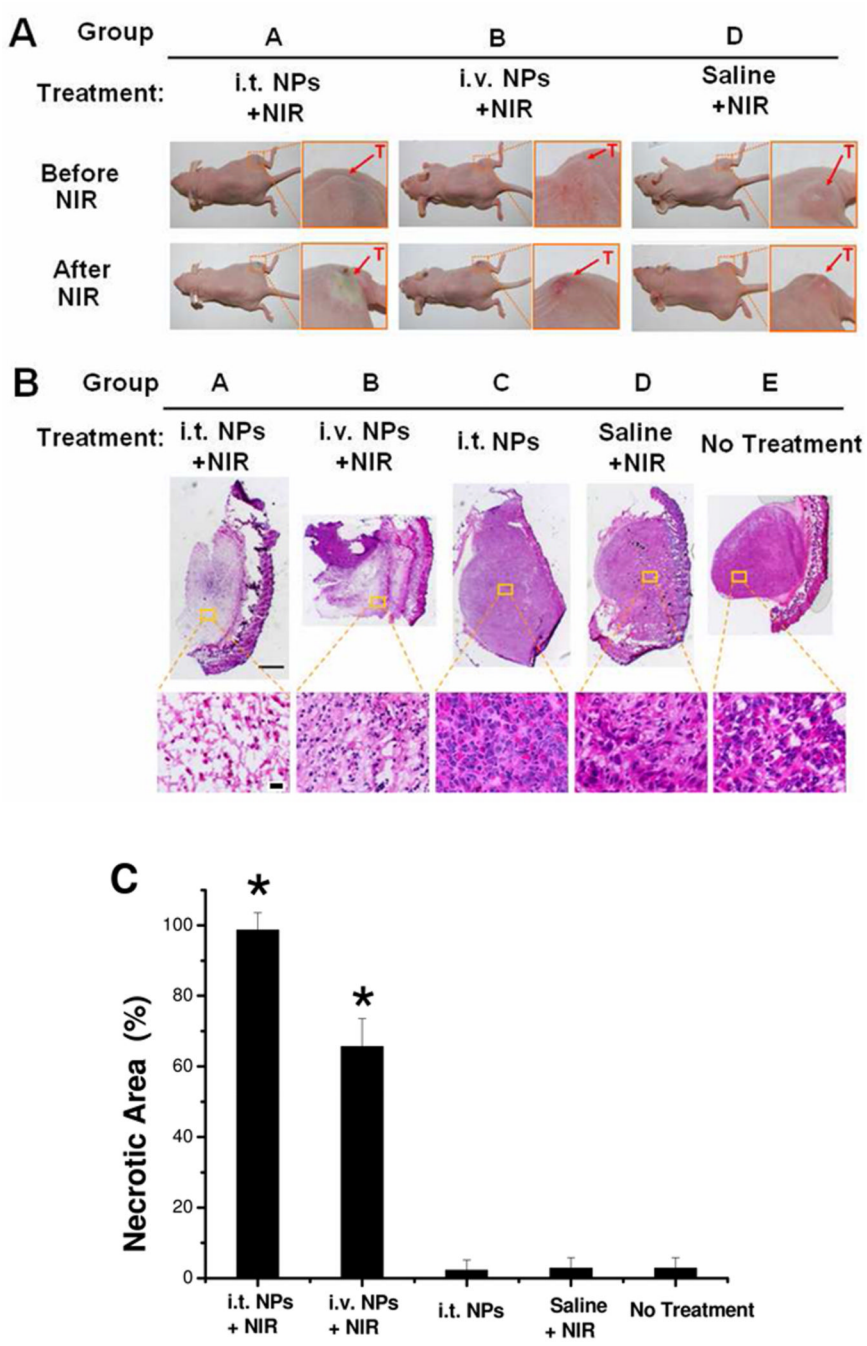

Figure 5.

PEG-CuS NPs induced photothermal destruction of U87 tumors *in vivo*. (A). Photographs of tumor-bearing mice before and at 24 h after NIR laser irradiation (12 W/cm^2 at 808 nm for 5 min). (B). Representative microphotograph of tumors removed at 24 h after NIR laser treatment. The tissues were cryosectioned into 5 μm slices and stained with H&E. Bar, top, 200 μm; Bar, bottle, 20 μm. (C). Quantitative analysis of percentage of necrosis zone induced by various treatments. The data were measured as a percentage of the whole tumor area. Asterisk indicates statistic significance compared to the no-treatment control ($p = 0.006$). Error bars, standard deviation ($n = 5$). NPs, CuS nanoparticles; NIR, near-infrared laser; T, tumor.

Table 1

Radiolabeling efficiency and stability of [^{64}Cu]-CuS NPs*

	Cit-[^{64}Cu]-CuS NPs	PEG-[^{64}Cu]-CuS NPs
CuS NPs	100%	100%
CuS NPs in PBS	87.3%	99.8%
CuS NPs in FBS	84.7%	99.2%

* Representative radio-instant thin-layer chromatograms after incubation in phosphate buffered saline (PBS) or 100% fetal bovine serum (FBS) at 37°C for 24 h.

Table 2

Pharmacokinetics parameters of Cit-[^{64}Cu]-CuS NPs and PEG-[^{64}Cu]-CuS NPs after intravenous injection in mice*

	$T_{1/2}\alpha$ (h)	$T_{1/2}\beta$ (h)	AUC (%ID h/mL)	Vd(ss) (mL)	Vc (mL)	CL (ml/h)	MRT (h)
Cit-[^{64}Cu]-CuS NPs	0.76±0.03	5.98±0.35	134.9±15.56	5.80±0.86	3.57+0.22	0.75±0.09	7.74±0.32
PEG-[^{64}Cu]-CuS NPs	0.71±0.36	6.06±1.58	213.7±32.36	3.79±0.85	2.39+0.56	0.48±0.07	8.05±1.90

Values are means ± standard deviations.

Abbreviations: $t_{1/2}\alpha$, blood distribution half-life; $t_{1/2}\beta$, blood terminal elimination half-life; AUC, area under the blood activity–time curve; Vd(ss), volume of distribution at steady-state; Vc, volume of distribution in the central compartment, CL, total body clearance; MRT, mean residence time.